Cell Communication and Signaling

RESEARCH

Open Access

Spinster homolog 2/S1P signaling ameliorates macrophage inflammatory response to bacterial infections by balancing PGE_2 production

Chao Fang[1†], Pan Ren[2†], Yejun He[1†], Yitian Wang[1†], Shuting Yao[1], Congying Zhao[2], Xueyong Li[2], Xi Zhang[3*], Jinqing Li[4*] and Mingkai Li[1*]

Abstract

Background Mitochondria play a crucial role in shaping the macrophage inflammatory response during bacterial infections. Spinster homolog 2 (Spns2), responsible for sphingosine-1-phosphate (S1P) secretion, acts as a key regulator of mitochondrial dynamics in macrophages. However, the link between Spns2/S1P signaling and mitochondrial functions remains unclear.

Methods Peritoneal macrophages were isolated from both wild-type and *Spns2* knockout rats, followed by non-targeted metabolomics and RNA sequencing analysis to identify the potential mediators through which Spns2/S1P signaling influences the mitochondrial functions in macrophages. Various agonists and antagonists were used to modulate the activation of Spns2/S1P signaling and its downstream pathways, with the underlying mechanisms elucidated through western blotting. Mitochondrial functions were assessed using flow cytometry and oxygen consumption assays, as well as morphological analysis. The impact on inflammatory response was validated through both in vitro and in vivo sepsis models, with the specific role of macrophage-expressed Spns2 in sepsis evaluated using *Spns2*$^{flox/flox}$*Lyz2-Cre* mice. Additionally, the regulation of mitochondrial functions by Spns2/S1P signaling was confirmed using THP-1 cells, a human monocyte-derived macrophage model.

Results In this study, we unveil prostaglandin E_2 (PGE_2) as a pivotal mediator involved in Spns2/S1P-mitochondrial communication. Spns2/S1P signaling suppresses PGE_2 production to support malate-aspartate shuttle activity. Conversely, excessive PGE_2 resulting from Spns2 deficiency impairs mitochondrial respiration, leading to intracellular

†Chao Fang, Pan Ren, Yejun He and Yitian Wang contributed equally to this work.

*Correspondence:
Xi Zhang
xizhang@fmmu.edu.cn
Jinqing Li
lijinqing@xjtu.edu.cn
Mingkai Li
mingkai@fmmu.edu.cn

Full list of author information is available at the end of the article

lactate accumulation and increased reactive oxygen species (ROS) generation through E-type prostanoid receptor 4 activation. The overactive lactate-ROS axis contributes to the early-phase hyperinflammation during infections. Prolonged exposure to elevated PGE_2 due to Spns2 deficiency culminates in subsequent immunosuppression, underscoring the dual roles of PGE_2 in inflammation throughout infections. The regulation of PGE_2 production by Spns2/S1P signaling appears to depend on the coordinated activation of multiple S1P receptors rather than any single one.

Conclusions These findings emphasize PGE_2 as a key effector of Spns2/S1P signaling on mitochondrial dynamics in macrophages, elucidating the mechanisms through which Spns2/S1P signaling balances both early hyperinflammation and subsequent immunosuppression during bacterial infections.

Keywords Macrophages, Spinster homolog 2, Sphingosine-1-phosphate, Prostaglandin E_2, Immunometabolism, Inflammatory response

Background

Cellular metabolism plays a pivotal role in shaping the homeostasis and function of immune cells [1]. Macrophages, the primary line of defense against pathogenic intrusions, undergo a significant metabolic transition from oxidative phosphorylation (OXPHOS) to aerobic glycolysis in the presence of bacterial infection [2]. This metabolic switch serves as a defining feature of macrophage activation and fuels the inflammatory response [3]. The manipulation of macrophage immunometabolism has been identified as a promising therapeutic avenue for combating infectious diseases [4].

Spinster homolog 2 (Spns2) functions as a membrane transporter facilitating the release of sphingosine-1-phosphate (S1P), which binds to five G protein-coupled receptors (S1PR1-5) to exert various biological effects [5]. Previous studies have indicated that the autocrine/paracrine S1P signaling mediated by macrophage-expressed Spns2 is essential for maintaining OXPHOS, with Spns2 deficiency leading to increased aerobic glycolysis even under basal conditions [6]. The metabolic switch orchestrated by Spns2/S1P signaling is closely linked to malate-aspartate shuttle (MAS) activity, which plays a key role in transferring electrons from NADH in the cytosol to the electron transport chain in the mitochondria [7]. Impaired MAS function results in decreased mitochondrial membrane potential ($\Delta\Psi m$), mitochondrial fragmentation, compromised OXPHOS, and enhanced aerobic glycolysis [8, 9]. Furthermore, the accumulation of intracellular lactate, a major glycolysis byproduct in Spns2-deficient (*Spns2*$^{-/-}$) macrophages, triggers oxidative stress by promoting mitochondrial reactive oxygen species (mtROS) generation, thereby fueling a pro-inflammatory response during bacterial infections through the lactate-ROS axis [10].

Being a crucial regulator of mitochondrial functions in macrophages, Spns2/S1P signaling holds promise as a potential therapeutic target for sepsis [6, 10]. Nevertheless, the intermediary mechanisms connecting Spns2/S1P signaling to mitochondrial functions remain elusive. Here, we have identified prostaglandin E_2 (PGE_2) as a metabolite that shows a significant difference between wild-type (WT) and *Spns2*$^{-/-}$ macrophages. Derived from arachidonic acid (AA), PGE_2 serves as a lipid signaling molecule with pivotal roles in inflammation and physiological processes [11]. AA is released from cellular membranes by phospholipase A_2 (PLA_2) enzymes and undergoes oxidation by cyclooxygenase (COX) enzymes to generate prostaglandins [12]. The biosynthesis of PGE_2 involves three synthases, namely microsomal PGE synthase-1 (mPGES-1), mPGES-2, and cytosolic PGE synthase (cPGES), among which mPGES-1 is prominently activated by diverse stimuli and is responsible for the majority of PGE_2 production [13]. Upon synthesis, PGE_2 binds to four E-type prostanoid receptors (EP1-4) in an autocrine/paracrine manner to initiate signal transduction, with EP2 and EP4 predominantly modulating the immune response in macrophages [11]. However, the precise role of PGE_2 as either a pro-inflammatory or anti-inflammatory mediator in macrophages remains controversial [14–19].

In the present study, we have identified Spns2/S1P signaling as an essential modulator of PGE_2 synthesis through the p38 mitogen-activated protein kinase (MAPK) cascade in macrophages. The heightened PGE_2 levels resulting from the deficiency of Spns2/S1P signaling dampened MAS activity and mitochondrial functions via EP4 activation. Blocking the PGE_2-EP4 pathway mitigated the lactate-ROS axis activity, consequently alleviating hyperinflammation during the initial stages of infection. Intriguingly, the excessive production of PGE_2 due to Spns2/S1P deficiency was correlated with the subsequent onset of immunosuppression, indicating the time-dependent dual roles of PGE_2 in modulating the immune response to bacterial challenges. Overall, our findings reveal the crucial roles of PGE_2 in bridging Spns2/S1P signaling with macrophage inflammatory response to bacterial infections.

Methods

Animals and sepsis models

WT and *Spns2* global knockout male Sprague-Dawley rats, aged 8 to 10 weeks and weighing 200 to 220 g, were utilized in this study [6, 20, 21]. To verify the specific role of macrophage-expressed Spns2 in sepsis, we mated $Spns2^{flox/flox}$ mice with *Lyz2-Cre* mice to obtain $Spns2^{flox/flox}$*Lyz2-Cre* ($Spns2\Delta^{Lyz2}$) mice. The transgenic mice were purchased from Cyagen Biosciences. Animals were housed in a specific pathogen-free environment before use. Ethical approval for all experimental procedures was obtained from the Animal Care and Use Committee of the Fourth Military Medical University.

To establish heat-killed *Escherichia coli* (*E. coli*)-induced septic rat models, *E. coli* (ATCC25922) was cultured overnight, washed with sterile saline, and adjusted to 2×10^9 colony-forming units (CFU)/ml in sterile saline. Subsequently, the bacterial suspension was heated at 68 ℃ for 30 min. Infection was induced by intraperitoneal injection of 0.3 ml/100 g of the prepared suspension. $Spns2^{-/-}$ models were treated with 1 ml of 10 μM S1P (Cayman Chemical, 62570), 1 μM EP2 antagonist PF-04418948 (TargetMOI, T3306) [22], or 1 μM EP4 antagonist ONO-AE3-208 (TargetMOI, TQ0290) [23] immediately after infection. WT and $Spns2^{-/-}$ rats in the control groups received 1 ml of sterile saline. For heat-killed *E. coli*-induced septic mouse models, the bacterial suspension was prepared at a concentration of 5×10^8 CFU/ml and administered intraperitoneally at 0.5 ml/100 g. A 0.2 ml dose of the treatment was administered to each group immediately following infection.

To establish cecal ligation and puncture (CLP) models, the cecum was exposed under aseptic conditions and ligated tightly at a distance of 1.5 cm for rats and 1 cm for mice with a 4−0 silk suture. Subsequently, the ligated cecum was punctured twice for rats and once for mice with an 18-gauge needle, and feces were gently extruded from the puncture sites. $Spns2^{-/-}$ rats were intraperitoneally injected with 2 ml of either 10 μM S1P, 1 μM PF-04418948, or 1 μM ONO-AE3-208 immediately after CLP. For $Spns2\Delta^{Lyz2}$ mice, 0.4 ml of the treatment was administered to each group. Maintenance doses, equivalent to half the initial volume, were given every 12-h. Control groups received an equal volume of sterile saline.

CFU counting

Rats were euthanized at 36-h post-CLP. The livers and spleens were aseptically harvested, weighed, homogenized in sterile saline, and plated on agar plates at suitable dilutions. After incubation for 18-h at 37 °C, CFU was quantified and shown as CFU/g.

Cell culture and stimulations

The isolation of peritoneal macrophages (PMs) was conducted as previously reported with adjustments [24]. Peritoneal cells were extracted by intraperitoneal injection of 10 ml ice-cold PBS, followed by centrifugation at 800 rpm for 5 min to collect the cell pellet. The cells were resuspended at a density of 5×10^6 cells/ml in a culture medium comprising DMEM supplemented with L-glutamine (Hyclone, SH30022.01), 10% fetal bovine serum (HyCyte, FBP-S001), 100 U/ml penicillin, and 100 μg/ml streptomycin (Gibco, 10378016). After incubating at 37 °C with 5% CO_2 for 1-h, non-adherent cells were gently washed away with PBS. Purified PMs were further incubated overnight before stimulation.

PMs were pre-treated with the following compounds for 1-h before analysis, unless otherwise stated: 5 μM Spns2 inhibitor SLF1081851 (MedChemExpress, HY-149004), 1 μM S1P, 100 nM PF-04418948, 100 nM ONO-AE3-208, 200 nM PGE_2 (TargetMOI, T5014), 2 μM S1PR1 antagonist W146 (Cayman Chemical, 10009109), 2 μM S1PR2 antagonist JTE013 (Cayman Chemical, 10009458), 2 μM S1PR3 antagonist TY-52,156 (TargetMOI, T17183), 2 μM S1PR4 antagonist CYM50358 (Tocris Bioscience, 4679), 5 μM S1PR1 agonist CYM5442 (TargetMOI, T2026), 5 μM S1PR2 agonist CYM5520 (TargetMOI, T22703), 5 μM S1PR3 agonist CYM5541 (TargetMOI, T3961), 5 μM S1PR4 agonist CYM50260 (TargetMOI, T15031), and 50 nM S1PR5 agonist A971432 (Cayman Chemical, 25326).

THP-1 cells were cultured at a density of 5×10^5 cells/ml in RPMI-1640 medium supplemented with L-glutamine, 10% fetal bovine serum, 100 U/ml penicillin, 100 μg/ml streptomycin, and 200 ng/ml phorbol 12-myristate 13-acetate (PMA, GLPBIO, GN10444) for 24-h. Adherent cells were washed 3 times with sterile PBS and treated after a 24-h recovery period.

LC-MS analysis

PMs were rinsed with ice-cold PBS, and around 5×10^6 cells were harvested and flash-frozen with liquid nitrogen. The samples were preserved in a -80 °C freezer until required. The metabolite extraction and subsequent LC-MS analysis were conducted by Majorbio Bio-Pharm Technology Co. Ltd. Briefly, the samples were treated with 400 μl of extraction solution (methanol: water=4:1 (v: v)) containing 0.02 mg/ml of L-2-chlorophenyl alanine, followed by low-temperature homogenization and ultrasonication, and incubated at -20 °C for 30 min. The supernatant was obtained through centrifugation at 13,000 g for 15 min at 4 °C. The samples were then subjected to LC-MS analysis using UHPLC-Q Exactive HF-X system (Thermo Fisher Scientific) equipped with an ACQUITY UPLC HSS T3 column (100 mm × 2.1 mm i.d., 1.8 μm). The injection volume was 2 μl, and the

column temperature was set at 40 ℃. The mass spectrometric signals were collected in both positive and negative modes, with a mass scanning range of 70–1050 m/z. For positive mode analysis, the mobile phases for chromatographic separation consisted of 0.1% formic acid in water (A) and 0.1% formic acid in acetonitrile (B). The negative mode analysis utilized mobile phases comprising 6.5mM NH_4HCO_3 in water (C) and 6.5mM NH_4HCO_3 in a mixture of 95% methanol and 5% water (D). The metabolites were identified through database searches, utilizing resources such as the HMDB (http://www.hmdb.ca/), Metlin (https://metlin.scripps.edu/), and the Majorbio Database. The data analysis was performed by using the Majorbio cloud platform (http://cloud.majorbio.com).

Gene expression

The RNA sequencing outcomes were derived from our prior investigations, which compared the gene expression patterns between WT and *Spns2*$^{-/-}$ PMs both before and after exposure to 10 ng/ml LPS (InvivoGen, Ultrapure LPS, *E. coli* 0111:B4) for 3-h [6]. The raw data have been deposited in the Sequence Read Archive database with the accession PRJNA904828 (https://www.ncbi.nlm.nih.gov/sra/PRJNA904828).

For the assays of quantitative PCR, total RNA was extracted using the SteadyPure Quick RNA Extraction Kit (Accurate Biotechnology, AG21023). Reverse transcription was conducted using Hifair® V one-step RT-gDNA digestion SuperMix (YEASEN, 11142ES). Quantitive PCR was performed using SYBR Green Premix Pro Taq HS qPCR Kit (Accurate Biotechnology, AG11739). Gene expression levels were normalized to *Arbp* for PMs and *hACTB* for THP-1 cells. The primer sequences used were as follows: *Tnfα*, 5'-TGGCGTGTTC ATCCGTTCT and 5'-TCAGCGTCTCGTGTGTTTCT; *Il-1β*, 5'-GGGATGATGACGACCTGCTA and 5'-CACT TGTTGGCTTATGTTCTGT; *Il-6*, 5'-CCCACCAGGAA CGAAAGTCAA and 5'-CATCAGTCCCAAGAAGGCA AC; *Ptges*, 5'-TGCAGGAGTGACCCAGATGT and 5'-T GTGAGGACCACGAGGAAATG; *Arbp*, 5'-TAGAGGG TGTCCGCAATGTG and 5'- CAGTGGGAAGGTGTAG TCAGTC; *hPTGES*, 5'-CCCAGTATTGCAGGAGCGAC and 5'-AAGTGCATCCAGGCGACAAA; *hACTB*, 5'- AA CTGGGACGACATGGAGAAA and 5'- GGATAGCAC AGCCTGGATAGCA.

Measurement of pro-inflammatory cytokines

Serum from the septic models and culture supernatant were gathered at indicated time points. The concentrations of TNFα (Proteintech, KE20018 and KE10002), IL-1β (Proteintech, KE20021), and IL-6 (ZCiBiO, ZC-36404) were assessed using enzyme-linked immunosorbent assay (ELISA) kits according to the manufacturers' instructions.

Measurement of PGE2

PMs were cultured overnight and the supernatant was collected. PMs were further stimulated with 10 ng/ml LPS and the supernatant was gathered after 6-h. The levels of PGE_2 were detected using the PGE_2 ELISA Kit-Monoclonal (Cayman, 514010) as per the manufacturer's instructions.

Western blot

Cells were lysed using RIPA Lysis Buffer (Proteintech, PR20035) supplemented with protease and phosphatase inhibitor cocktails (Mei5bio, MF182-plus and MF183). Subsequently, the protein was separated via 10% SDS-PAGE electrophoresis and transferred onto PVDF membranes (Millipore, ISEQ00010). Following blocking with 5% skim milk or bovine serum albumin (BSA) at room temperature for 2-h, the PVDF membranes were incubated with primary antibodies overnight at 4 °C. Anti-Drp1 (A16661), anti-Opa1 (A9833), anti-Slc25a12 (A11688), anti-Slc25a13 (A12557), and anti-β-Actin (AC026) were purchased from ABclonal Technology. Anti-$cPLA_2$ (2832), anti-p-$cPLA_2^{Ser505}$ (2831) were purchased from Cell Signaling Technology. Anti-p38 (14064-1-AP), anti-p-p38$^{Thr180/Tyr182}$ (28796-1-AP), anti-JNK (24164-1-AP), anti-p-JNK^{Tyr185} (80024-1-RR), anti-ERK1/2 (11257-1-AP), and anti-ERK1/2$^{Thr202/Tyr204}$ (80031-1-RR) were purchased from Proteintech. After incubation with HRP-conjugated secondary antibodies for 1-h at room temperature, the membranes were visualized using an ECL substrate (AccuRef Scientific, AP0081). The images were analyzed using ImageJ v.1.53k.

Transmission electron microscopy (TEM)

PMs were rinsed with ice-cold PBS and harvested by cell scrapers. After centrifugation, cell pellets were pre-fixed with 3% glutaraldehyde, and subsequently post-fixed with 1% osmium tetroxide. The samples underwent a process of dehydration, infiltration, and embedding. Ultrathin sections were stained with uranyl acetate and lead citrate. The observations were conducted utilizing a JEM-1400-FLASH transmission electron microscope. Mitochondrial length was analyzed using ImageJ v.1.53k.

Flow cytometry

MitoSOX™ Red (Invitrogen, M36008) fluorescent probe was applied at a concentration of 5 μM to quantify the levels of mtROS. For the detection of total cellular ROS, CellROX® Orange Reagent (Invitrogen, C10443) was used at a concentration of 5 μM. Mitochondria were labeled with the Δψm-independent dye CytoFix™ MitoRed (AAT Bioquest, 23200) at a 1:200 dilution to represent mitochondrial mass. The Δψm-dependent dye MitoTracker™ Red CMXRos (Invitrogen, M7512) was used at a concentration of 250 nM to reflect overlaid Δψm. Following

staining at 37 °C with 5% CO_2 for 30 min, cells were detached from the culture plates with ice-cold PBS containing 1 mM EDTA. The Mean fluorescent intensity (MFI) was quantified by flow cytometry and analyzed using FlowJo v.10. The ratio of $MFI_{MitoTracker^{™} Red}$ to $MFI_{CytoFix^{™} MitoRed}$ was calculated to represent the average Δψm of individual mitochondria [25].

Oxygen consumption rate (OCR)

The OCR was assessed using a Mitochondrial Stress Test Complete Assay Kit (Abcam, ab232857) as previously described [6]. Briefly, PMs, seeded in 96-well flat clear bottom black microplates (Corning), were pre-treated with the designated stimuli for 1-h. Then, the culture medium was replaced with a fresh medium containing each stimulus and extracellular O_2 probe. A final concentration of 1.5 μM oligomycin, 2.5 μM carbonyl cyanide-4-(trifluoromethoxy) phenylhydrazone (FCCP), or a combination of 1 μM antimycin A and 1 μM rotenone was added, respectively. Following the addition of 100 μl pre-warmed mineral oil to each well, the fluorescence intensity was promptly measured every 2 min for 30 min. The slopes (m) derived from the signal profiles were indicative of OCR. The basal respiration rate was determined by calculating $m_{untreated}$ - $m_{antimycin\ A}$. The maximal respiration rate was calculated as m_{FCCP} - $m_{antimycin\ A}$. ATP-coupled oxygen consumption was assessed as $m_{untreated}$ - $m_{oligomycin}$, while the non-ATP-coupled oxygen consumption (proton leak) was determined as $m_{oligomycin}$ - $m_{antimycin\ A}$. The data were normalized by protein quantification using the Enhanced BCA Protein Assay Kit (Beyotime, P0010).

Measurement of intracellular lactate

PMs were pre-treated with the indicated stimuli for 1-h, followed by washing with ice-cold PBS and lysis using Cell lysis buffer for Western and IP (Beyotime, P0013). The intracellular lactate levels were assessed using the Lactate Colorimetric Assay Kit (Nanjing Jiancheng Bioengineering Institute, A019-2-1) as per the manufacturer's instructions. The data were normalized by protein quantification.

Measurement of oxidative stress

The cellular oxidative stress was evaluated by determining the activities of both total superoxide dismutase (Beyotime, S0101) and catalase (Beyotime, S0051) in the cell lysate following the manufacturer's instructions. The data were normalized by protein quantification.

Detection of plasma leakage and edema

Evans blue (Solarbio, E8010) was injected via the tail vein at a dose of 20 mg/kg. After 30 min, rats were euthanized and immediately perfused with ice-cold saline. Approximately 100 mg (wet weight) of liver and spleen tissue were collected and dried in an incubator at 65 °C. After 3 days, the dry weight was measured, and the wet-to-dry weight ratio was calculated. The dehydrated samples were then incubated with formamide at room temperature for 3 days to extract Evans blue. The absorbance of the supernatant was measured by spectrophotometry at 620 nm (OD_{620}).

Statistical analysis

The results were presented as means±s.e.m. Statistical differences were determined using GraphPad Prism v.8.4.3. Unpaired Student's t-test was used for comparisons between the two groups. For comparisons among multiple groups, one-way ANOVA with Sidak's correction for multiple comparisons was employed. Log-rank test adjusted by the Bonferroni method was conducted for survival analysis. P values less than 0.05 were considered statistically significant.

Results

Spns2/S1P deficiency elevates AA metabolism and PGE_2 formation in PMs

To explore the metabolites potentially implicated in Spns2/S1P-mitochondrial communication, we compared the metabolic profiles of WT and *Spns2*$^{-/-}$ PMs. Partial least squares-discriminant analysis (PLS-DA) unveiled distinct metabolic patterns between the two genotypes (Supplementary Fig. 1A and B). Totally, 98 distinct metabolites were identified (Fig. 1A), with the Kyoto Encyclopedia of Genes and Genomes (KEGG) enrichment analysis indicating heightened activities of glycerophospholipid metabolism and AA metabolism in *Spns2*$^{-/-}$ PMs (Fig. 1B). Notably, AA and its derivatives were found to be enriched in *Spns2*$^{-/-}$ PMs, accompanied by elevated levels of lysophospholipids (Fig. 1A and C). These metabolic alterations suggested an augmented activation of PLA_2 in the absence of Spns2, which plays essential roles in glycerophospholipid metabolism and arachidonic acid release [12]. We determined that inhibition of Spns2-mediated S1P release in WT PMs by SLF1081851 potentiated cytosolic PLA_2 ($cPLA_2$) activity, while supplementation of S1P decreased the level of p-$cPLA_2^{Ser-505}$ in *Spns2*$^{-/-}$ PMs (Fig. 1D and E). Furthermore, we observed the activation of key mitogen-activated protein kinases (MAPKs) and determined that Spns2/S1P signaling repressed $cPLA_2$ activity through the p38-MAPK pathway rather than the ERK1/2- or JNK-MAPK pathways (Fig. 1D and E). This finding was further confirmed by using the THP-1 cell line, a human monocyte-derived macrophage model, where inhibiting SPNS2 function with SLF1081851 significantly enhanced the activation levels of P38 and $cPLA_2$, suggesting that this

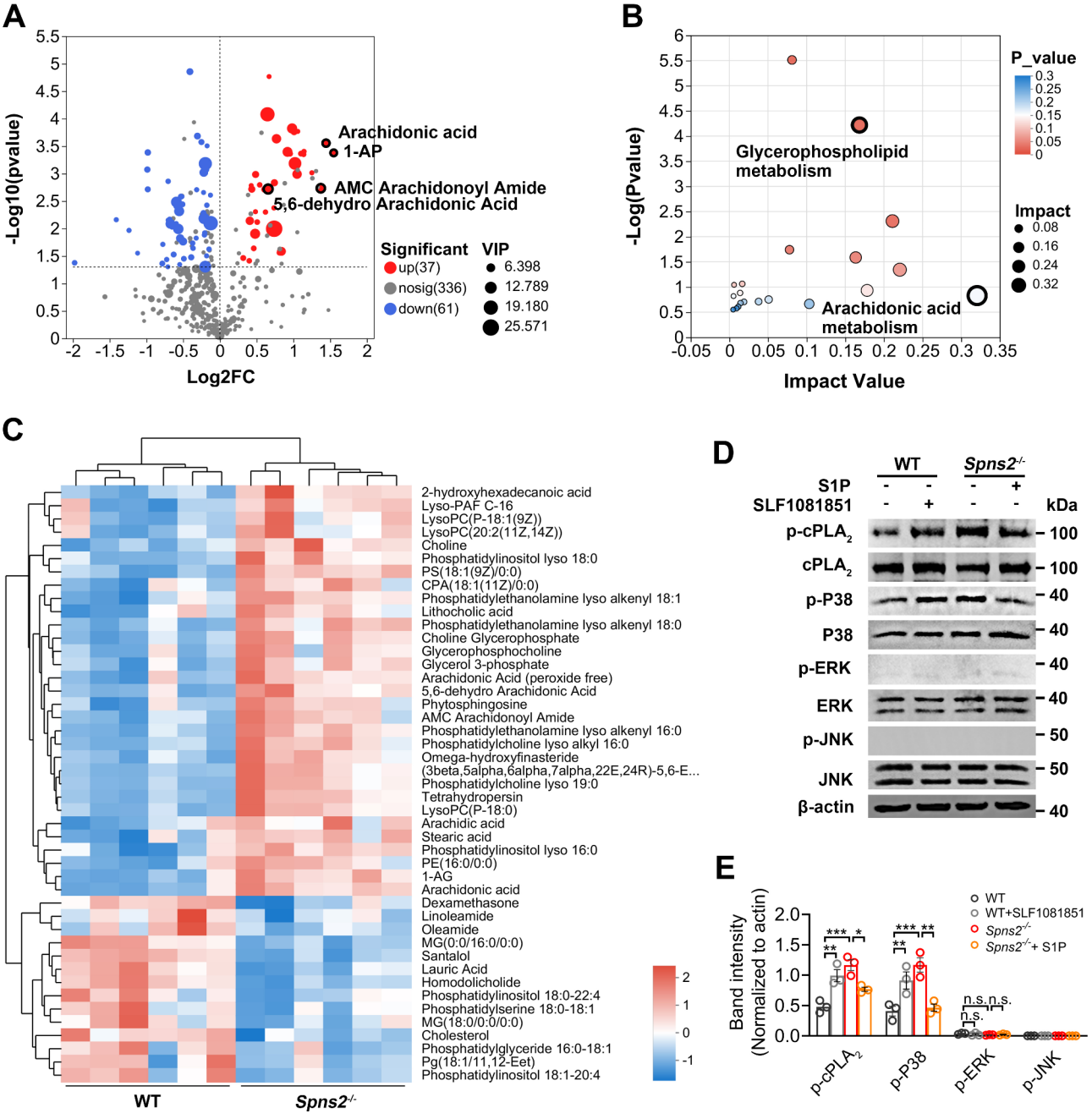

Fig. 1 Spns2/S1P deficiency enhances AA metabolism through p38-MAPK mediated cPLA$_2$ activation **(A)** The volcano plot illustrates the identification of 98 distinct metabolites between WT and *Spns2*$^{-/-}$ PMs. AA and its derivatives are enriched in *Spns2*$^{-/-}$ PMs. **(B)** KEGG enrichment analysis indicates elevated activities of glycerophospholipid metabolism and AA metabolism in *Spns2*$^{-/-}$ PMs. **(C)** The heat map of the differential metabolites highlights the accumulation of AA derivatives and lysophospholipids in *Spns2*$^{-/-}$ PMs. $N=6$ biological replicates (**A** to **C**). (**D**, **E**) Deficient Spns2/S1P signaling enhances p38-MAPK mediated cPLA$_2$ activation. $N=3$ biological replicates. Data are presented as mean ± s.e.m. **(E)**. *P* values were determined by one-way ANOVA with Sidak's correction for multiple comparisons **(E)**. *$P<0.05$; **$P<0.01$; ***$P<0.001$; n.s., not significant

effect may be conserved across species (Supplementary Fig. 2A).

Subsequently, we analyzed the changes in gene expression of key enzymes involved in AA metabolism to anticipate the eicosanoid molecules influenced by Spns2/S1P signaling. While the transcriptional levels of COX enzymes and cytochrome P450 remained largely unchanged, a notable decrease was observed in the expression of *Alox5*, which encodes a pivotal enzyme involved in the synthesis of leukotrienes [26], within *Spns2*$^{-/-}$ PMs (Fig. 2A). This observation implies a diminished contribution of leukotrienes production in

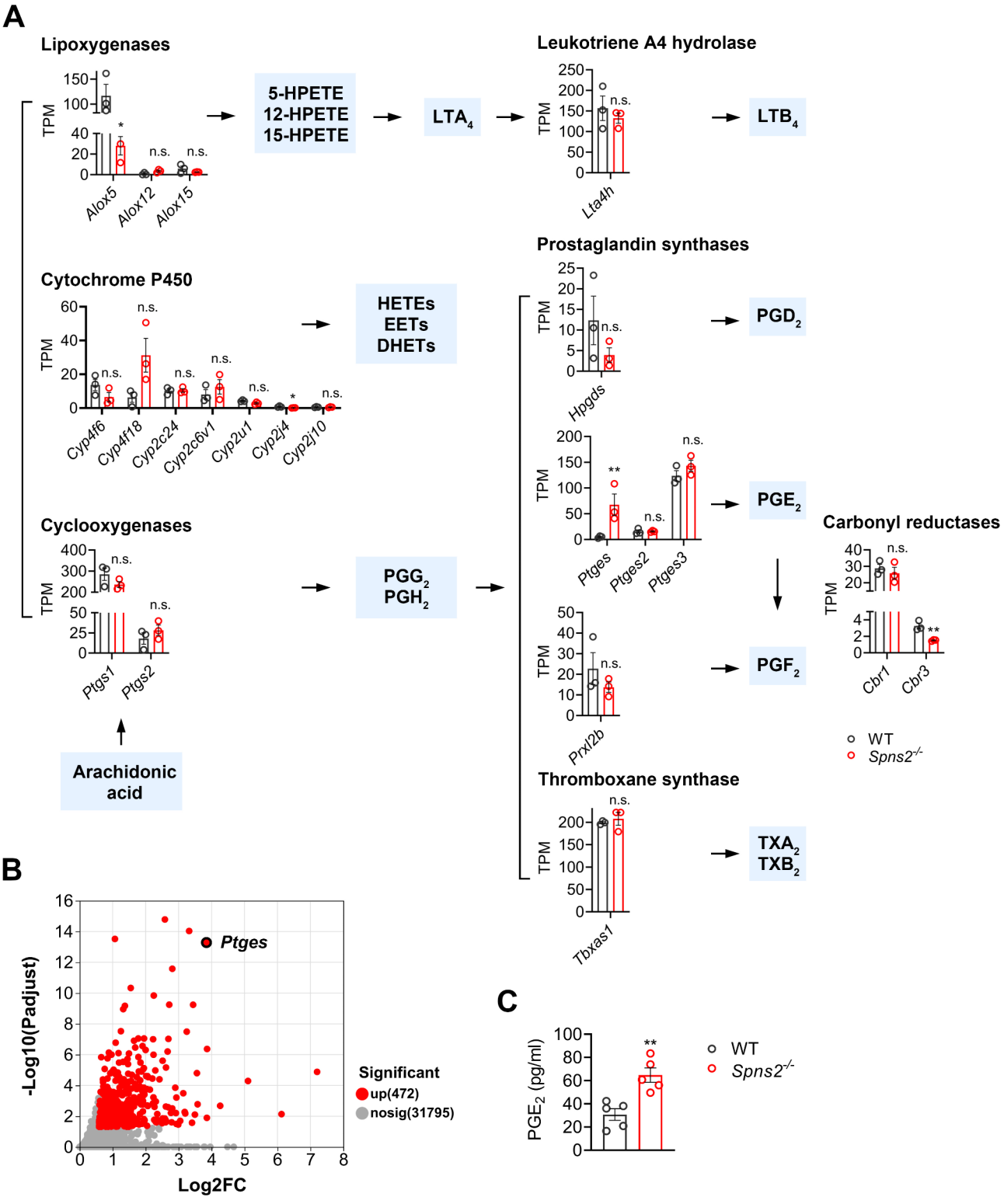

Fig. 2 Altered AA metabolism promotes PGE_2 production in *Spns2*$^{-/-}$ PMs **(A)** The flow diagram illustrating AA metabolism reveals a significant elevation in the gene expression of *Ptges*, encoding mPGES-1, in *Spns2*$^{-/-}$ PMs. TPM, transcripts per kilobase of exon model per million mapped reads. **(B)** The volcano plot of up-regulated genes in *Spns2*$^{-/-}$ PMs highlights the significant alteration in *Ptges* expression. $N = 3$ biological replicates (**A** and **B**). (**C**) *Spns2*$^{-/-}$ PMs release elevated levels of PGE_2 under resting conditions. $N = 5$ biological replicates. Data are presented as mean ± s.e.m. (**A** and **C**). *P* values were determined by unpaired *t*-test. *$P < 0.05$; **$P < 0.01$; ***$P < 0.001$; n.s., not significant

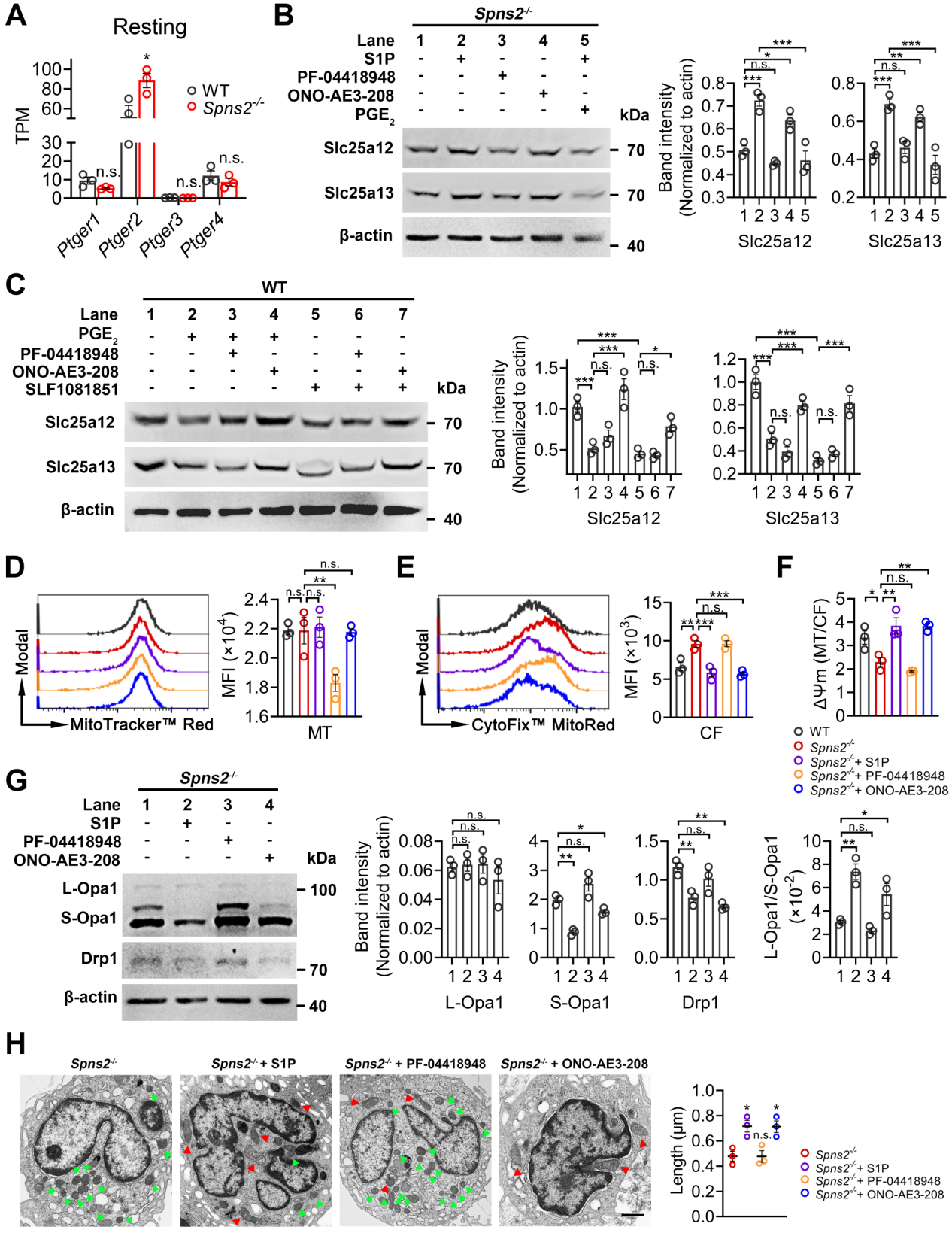

Fig. 3 (See legend on next page.)

(See figure on previous page.)

Fig. 3 Overproduction of PGE_2 impairs MAS activity and mitochondrial dynamics **(A)** Gene expression of E-type prostanoid receptors in resting PMs. TPM, transcripts per kilobase of exon model per million mapped reads. $N = 3$ biological replicates. **(B)** Inhibition of EP4 with ONO-AE3-208, but not EP2 with PF-04418948, elevates the protein levels of MAS components Slc25a12 and Slc25a13 in *Spns2*$^{-/-}$ PMs. $N = 3$ biological replicates. **(C)** EP4 activation contributes to the downregulation of Slc25a12 and Slc25a13 in WT PMs exposed to either PGE_2 or Spns2 inhibitor SLF1081851. $N = 3$ biological replicates. (**D**, **E**) Flow cytometry analysis of overlaid Δψm probed by MitoTracker™ Red (MT, D) and mitochondrial mass probed by CytoFix™ MitoRed (CF, E). MFI, mean fluorescent intensity. **(F)** Inhibition of EP4 restores the average Δψm (calculated by the ratio of MT/CF) in *Spns2*$^{-/-}$ PMs. $N = 3$ biological replicates (**D** to **F**). **(G)** EP4 inhibition modulates the expression of mitochondrial dynamics-related proteins, promoting mitochondrial fusion in *Spns2*$^{-/-}$ PMs. $N = 3$ biological replicates. **(H)** Transmission electron microscopy reveals that EP4 inhibition facilitates mitochondrial fusion in *Spns2*$^{-/-}$ PMs. Scale bar = 1 μm. Arrowheads indicate fused (red) and fragmented (green) mitochondrial morphology. $N = 3$ biological replicates. Data are presented as mean ± s.e.m. *P* values were determined by unpaired *t*-test **(A)** and one-way ANOVA with Sidak's correction for multiple comparisons (**B** to **H**). $^{*}P < 0.05$; $^{**}P < 0.01$; $^{***}P < 0.001$; n.s., not significant

the arachidonic acid metabolism orchestrated by Spns2/S1P signaling. Interestingly, the expression of *Ptges*, responsible for mPGES-1 synthesis, exhibited a substantial increase of approximately 10-fold in *Spns2*$^{-/-}$ PMs (Fig. 2A and B). Consistent with the pivotal role of mPGES-1 in PGE_2 synthesis [13], we observed elevated levels of PGE_2 production by *Spns2*$^{-/-}$ PMs (Fig. 2C). These findings suggest that PGE_2 formation serves as the predominant pathway for AA metabolism in the context of impaired Spns2/S1P signaling.

Excessive activation of PGE2-EP4 hampers MAS functions and causes mitochondrial fission

Next, we investigated whether the heightened production of PGE_2 contributed to the metabolic remodeling observed in *Spns2*$^{-/-}$ PMs. Consistent with prior findings [11], we determined that EP2 and EP4 were predominately expressed in resting PMs (Fig. 3A). In *Spns2*$^{-/-}$ PMs, inhibition of EP4 with ONO-AE3-208, but not EP2 with PF-04418948, resulted in elevated protein levels of MAS components Slc25a12 and Slc25a13 (Fig. 3B, lanes 1, 3, and 4). Furthermore, the enhancement of MAS through S1P supplementation was hindered by concurrent PGE_2 treatment (Fig. 3B, lanes 1, 2, and 5). In WT PMs, PGE_2 exposure suppressed the expression of Slc25a12 and Slc25a13, which could be reversed specifically by blocking EP4, but not EP2 (Fig. 3C, lanes 1 to 4). The dampening effect on MAS could also be induced by impeding S1P release through Spns2 inhibition, a process reliant on EP4 activation (Fig. 3C, lanes 5 to 7). These results underscore the crucial role of PGE_2-EP4 in bridging Spns2/S1P signaling and MAS functions.

Compromised MAS functions result in a decline in mitochondrial ΔΨm [6, 8, 9]. In *Spns2*$^{-/-}$ PMs, while the fluorescence intensities of MitoTracker™ Red (a probe dependent on ΔΨm) were comparable across groups (Fig. 3D), treatment with either EP4 blockade or S1P supplementation significantly decreased the mitochondrial mass, as indicated by CytoFix™ MitoRed (a probe independent of ΔΨm) (Fig. 3E). Consequently, the average ΔΨm of *Spns2*$^{-/-}$ PMs was restored by either EP4 inhibition or S1P treatment (Fig. 3F). The alterations in mitochondrial mass reflected changes in mitochondrial dynamics [27]. Further exploration into the key proteins involved in mitochondrial fusion and fission processes [28] revealed that the restoration of ΔΨm, triggered by EP4 inhibition and S1P treatment, suppressed the cleavage of long-form Opa1 (L-Opa1) into short-form Opa1 (S-Opa1), which is regulated by the potential-dependent protease Oma1 [29], indicating mitigated inner mitochondrial membrane fission (Fig. 3G). Moreover, EP4 inhibition and S1P treatment resulted in decreased levels of Drp1 (Fig. 3G), which is known to promote outer mitochondrial membrane fission [30]. Consequently, EP4 inhibition and S1P treatment facilitated mitochondrial fusion in *Spns2*$^{-/-}$ PMs (Fig. 3H), signifying the restoration of mitochondrial function.

We investigated the impact of PGE_2 on MAS functions and mitochondrial dynamics in THP-1 cells. PGE_2 treatment suppressed the expression of SLC25A12 and SLC25A13, an effect that could be reversed by EP4 blockade (Supplementary Fig. 2B). Additionally, PGE_2 elevated the levels of DRP1 and S-OPA1 in an EP4-dependent manner, indicating a pro-fission effect (Supplementary Fig. 2B). Consistently, PGE_2-EP4 signaling contributed to the decrease in average ΔΨm (Supplementary Fig. 2C to E). These results underscore the critical role of PGE_2 in regulating MAS functions and mitochondrial dynamics in macrophages under resting conditions.

EP4 blockade suppresses the lactate-ROS axis and attenuates hyperinflammation in *Spns2*$^{-/-}$ PMs

We have established that the excessive activation of the PGE_2-EP4 pathway accounted for mitochondrial fission in the context of Spns2 deficiency. Correspondingly, blocking EP4 and S1P treatment effectively restored the basal and maximal respiration, along with ATP-coupled oxygen consumption in *Spns2*$^{-/-}$ PMs (Fig. 4A and B), indicating that Spns2/S1P signaling enhanced OXPHOS by inhibiting PGE_2-EP4 activation. Elevated OXPHOS resulted in reduced intracellular lactate accumulation (Fig. 4C), which is known to positively drive the generation of mitochondrial ROS (mtROS) in macrophages [6, 10]. Consequently, EP4 blockade diminished mtROS production (probed by MitoSOX™ Red), aligning with the alterations in mitochondrial functions in *Spns2*$^{-/-}$ PMs

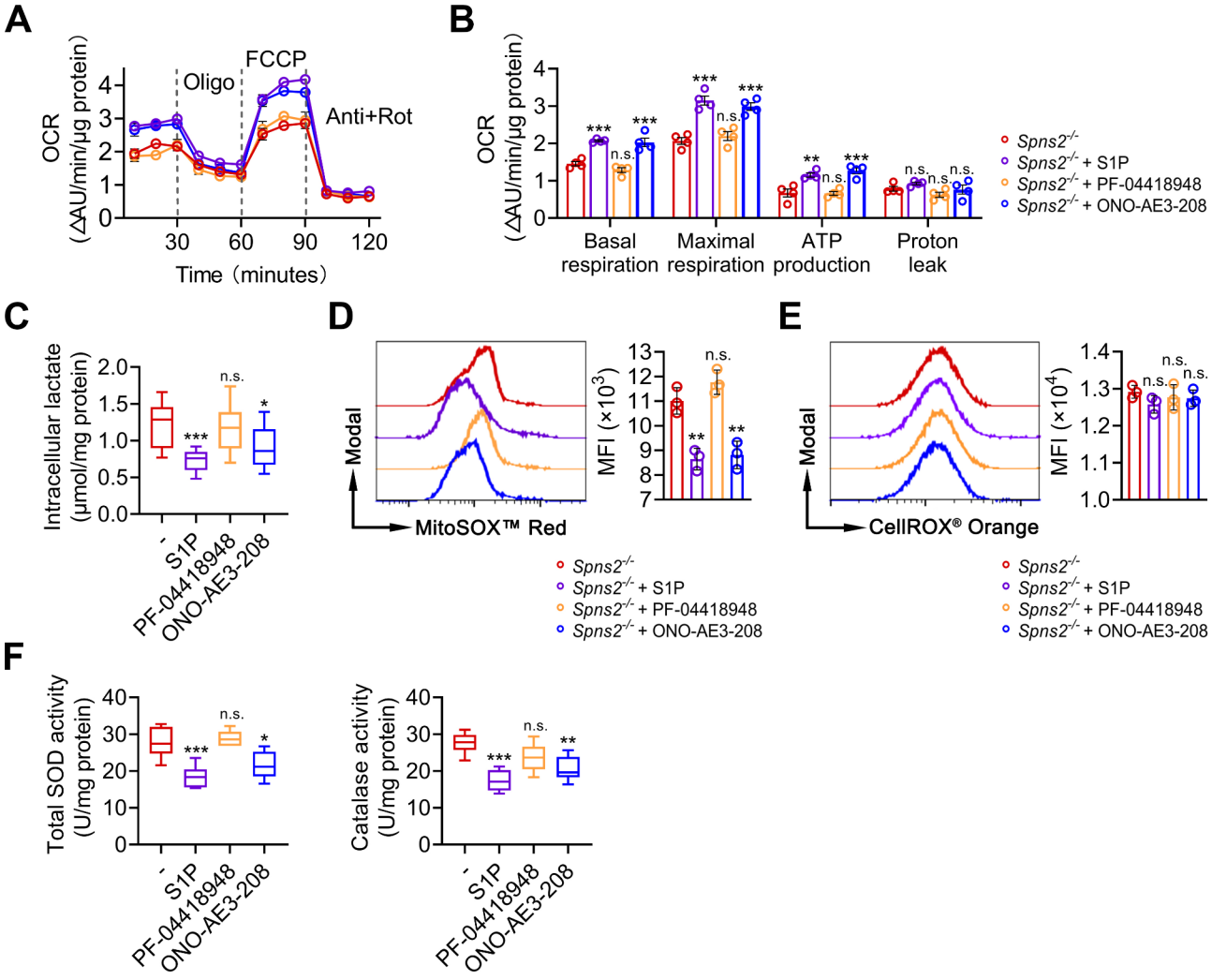

Fig. 4 Excessive EP4 activation impairs mitochondrial respiration and increases oxidative stress in *Spns2*$^{-/-}$ PMs **(A)** Blocking EP4 with ONO-AE3-208 increases the oxygen consumption rates (OCR) in *Spns2*$^{-/-}$ PMs. **(B)** Quantitative analysis of basal respiration, maximal respiration, ATP production, and proton leakage reveal the restoration of mitochondrial respiration following EP4 blockade. $N = 4$ biological replicates (**A** and **B**). **(C)** EP4 inhibition reduces intracellular lactate levels in *Spns2*$^{-/-}$ PMs. $N = 12$ biological replicates. **(D)** Flow cytometry analysis reveals a decrease in MitoSOX™ Red-probed mtROS generation in ONO-AE3-208-treated *Spns2*$^{-/-}$ PMs. $N = 3$ biological replicates. **(E)** Total intracellular ROS probed by CellROX® Orange remains comparable among each group. $N = 3$ biological replicates. **(F)** EP4 inhibition diminishes the activities of total superoxide dismutase (SOD) and catalase, indicating alleviated oxidative stress in *Spns2*$^{-/-}$ PMs. $N = 6$ biological replicates. Data in the panels **A**, **B**, **D**, and **E** are presented as mean ± s.e.m. In panels **C** and **F**, the central bands represent the median values, the boxes represent the distance between the third and the first quartile, and the whiskers represent the ranges between the minimum and maximum values. *P* values were determined by one-way ANOVA with Sidak's correction for multiple comparisons. $^{*}P < 0.05$; $^{**}P < 0.01$; $^{***}P < 0.001$; n.s., not significant

(Fig. 4D). While the overall intracellular ROS levels (probed by CellROX® Orange) displayed no significant differences among the groups (Fig. 4E), the mitigation of oxidative stress in *Spns2*$^{-/-}$ PMs through EP4 inhibition was evidenced by reduced activities of total superoxide dismutase (SOD) and catalase (Fig. 4F). Similarly, EP4 blockade attenuated mtROS production in PGE_2-treated THP-1 cells (Supplementary Fig. 2F). These findings indicate that EP4 blockade restores OXPHOS in Spns2/S1P-deficient macrophages and suppresses the activity of the lactate-ROS axis under basal conditions.

The excessive activity of the lactate-ROS axis in *Spns2*$^{-/-}$ PMs triggers hyperinflammation during the initial phase of bacterial infections [6, 10]. The restored metabolic state induced by EP4 inhibition attenuated the generation of mtROS and total intracellular ROS in LPS-exposed *Spns2*$^{-/-}$ PMs (Fig. 5A and B). Consequently, the suppressed lactate-ROS axis resulted in reduced gene expression of inflammatory cytokines 3-h post-LPS challenge (Fig. 5C). The immunomodulatory effect of EP4 inhibition was further corroborated in sepsis models triggered by intraperitoneal injection with heat-killed *E. coli* (Fig. 5D). EP4 inhibition alleviated hyperinflammation in

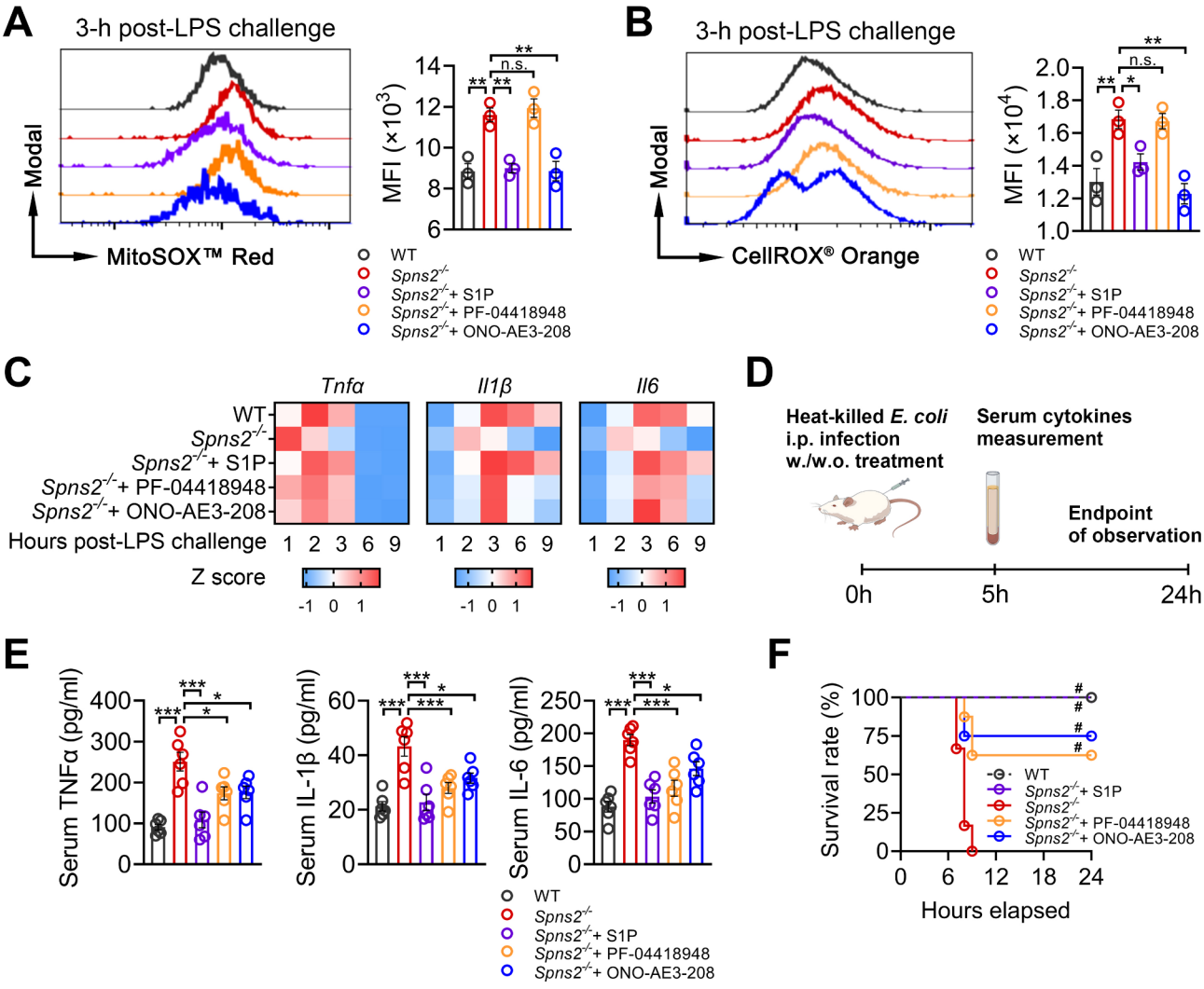

Fig. 5 PGE_2 contributes to the early-phase hyperinflammation during bacterial infections (**A**, **B**) Flow cytometry analysis shows reduced mtROS generation probed by MitoSOX™ Red **(A)** and decreased total intracellular ROS probed by CellROX® Orange **(B)** in ONO-AE3-208-treated *Spns2*$^{-/-}$ PMs at 3-h post-LPS challenge. $N = 3$ biological replicates (**A** and **B**). **(C)** EP4 blockade reduces the gene expression of inflammatory cytokines within 3-h post-LPS challenge due to the suppression of the lactate-ROS axis. Notably, EP2 blockade also attenuates the early-phase hyperinflammation, possibly via a mechanism independent of the lactate-ROS axis. Both EP2 and EP4 blockade partially restore the suppressed gene expression of inflammatory cytokines in *Spns2*$^{-/-}$ PMs after 6-h post-LPS challenge. $N = 3$ biological replicates. **(D)** Schematic of the in vivo experiments using heat-killed *E. coli*-induced peritoneal infection models. (E, F) Both EP2 and EP4 inhibition alleviate hyperinflammation **(E)** and significantly improve survival rates **(F)** in *Spns2*$^{-/-}$ sepsis models triggered by intraperitoneal infection with heat-killed *E. coli*. $N = 6$ biological replicates for cytokine measurement. $N = 6$ to 8 biological replicates for survival analysis. Data are presented as mean ± s.e.m. (**A**, **B**, and **E**) and percentage **(F)**. *P* values were determined by one-way ANOVA with Sidak's correction for multiple comparisons (**A**, **B**, and **E**) and log-rank test adjusted by the Bonferroni method **(F)**. $^*P < 0.05$; $^{**}P < 0.01$; $^{***}P < 0.001$; n.s., not significant. # indicates *P* value is less than the Bonferroni-corrected threshold

Spns2$^{-/-}$ sepsis models and significantly reduced mortality (Fig. 5E and F). These results suggest that PGE_2-EP4 signaling enhances the intensity of inflammatory response through the lactate-ROS axis. Interestingly, we noted comparable mitigating effects of EP2 inhibition on hyperinflammation, both in vitro and in vivo (Fig. 5C to F). Nevertheless, the impact of EP2 inhibition was unrelated to the lactate-ROS axis (Fig. 5A and B), suggesting a separate mechanism by which PGE_2 modulates immune response in PMs. Overall, these findings highlight the pro-inflammatory functions of PGE_2 in macrophages during the early phase of bacterial infections.

Overproduction of PGE_2 accounts for the onset of immunosuppression in *Spns2*$^{-/-}$ PMs

Despite the hyperinflammation observed during the early stages of infection, the rapid onset of immunosuppression is a prominent feature of immune response in the absence of Spns2/S1P signaling (Fig. 5C). We noticed a significant upregulation in the gene expression of *Ptges* in

Spns2$^{-/-}$ PMs even following the LPS challenge (Fig. 6A). Our findings indicate that the initial excessive production of PGE_2 in the context of Spns2 deficiency contributes to hyperinflammation, while the elevated levels of PGE_2 at 6-h post-LPS challenge suggest its potential involvement in the later stages of infection (Fig. 6B). In activated PMs, EP2 and EP4 remained the predominately expressed PGE_2 receptors (Fig. 6C). Inhibition of either EP2 or EP4 partially restored the suppressed gene expression of inflammatory cytokines in *Spns2*$^{-/-}$ PMs after 6-h (Fig. 5C). We measured the release of TNFα and IL-6 in the supernatant within 12-h, and the results were consistent with the gene expression patterns described above (Fig. 6D). These findings suggest that the immunomodulatory effects of PGE_2 may vary over time. Specifically, PGE_2 could induce immunosuppression by excessively stimulating EP2 and EP4 as the infection progresses.

In the sepsis models induced by cecal ligation and puncture (CLP), none of the *Spns2*$^{-/-}$ rats survived beyond 24-h post-infection (Fig. 6E and F). This outcome could be linked to immunosuppression, a phenomenon previously documented [6]. Upon blocking EP2 and EP4, there was a restoration of macrophage immune response observed in vitro (Figs. 5C and 6D). Consequently, the in vivo treatment led to a significant improvement in the survival rates of *Spns2*$^{-/-}$ CLP models (Fig. 6F). It was noted that the majority of mortalities occurred between 24 and 48-h post-infection in the WT group and the *Spns2*$^{-/-}$ groups treated with either EP2 or EP4 blocker. However, the causes of death differed among these groups. The levels of serum cytokines at 36-h post-infection indicated that the immune response in *Spns2*$^{-/-}$ CLP models was partially restored by either EP2 or EP4 inhibition (Fig. 6G). However, such restoration was limited in intensity compared to WT and S1P-treated *Spns2*$^{-/-}$ groups. Additionally, the number of colony-forming units (CFU) in the livers and spleens of both EP2- and EP4-inhibited *Spns2*$^{-/-}$ groups was higher than in the other groups (Fig. 6H). These results indicated that *Spns2*$^{-/-}$ CLP models treated with either EP2 or EP4 blocker succumbed to overwhelming bacterial loads due to an inadequate immune response, whereas the mortality in the WT and S1P treated *Spns2*$^{-/-}$ groups predominantly resulted from hyperinflammation.

However, since PGE_2 has been reported to enhance endothelial cell barrier function [31], the observed difference might be attributed to increased vascular permeability resulting from EP2 or EP4 blockade. To investigate this, we collected spleen and liver samples from rats that survived 30 to 36-h after CLP and assessed plasma leakage and edema using Evans blue extravasation and the wet-to-dry weight ratio (Supplementary Fig. 3A and B). However, no significant differences were observed among the groups. In sepsis, plasma leakage and edema are complex processes influenced by multiple factors, such as nitric oxide release, hyperinflammation, and bacterial virulence, which may mask the effects of EP2 or EP4 blockade on vascular permeability.

To further clarify the key role of macrophage-expressed Spns2 in sepsis, we used *Spns2*$^{flox/flox}$*Lyz2-Cre* (*Spns2Δ*^{Lyz2}) mice to specifically knock out *Spns2* in macrophages. In sepsis models of *Spns2Δ*^{Lyz2} mice, we observed similar outcomes to those in global *Spns2* knockout rats. First, intraperitoneal injection of heat-killed *E. coli* in *Spns2Δ*^{Lyz2} mice triggered a stronger inflammatory response and higher mortality, while blocking EP2 or EP4 alleviated hyperinflammation, thereby improving survival (Supplementary Fig. 4A to C). Additionally, the *Spns2Δ*^{Lyz2} CLP model exhibited higher mortality (Supplementary Fig. 4D and E). Consistent with previous findings, *Spns2Δ*^{Lyz2} mice showed a significantly dampened inflammatory response 12 to 16 h after CLP, indicating the onset of immunosuppression (Supplementary Fig. 4F). EP2 or EP4 blockade partially restored the inflammatory response in *Spns2Δ*^{Lyz2} mice and improved survival rates (Supplementary Fig. 4E and G). Overall, PGE_2 serves as a pivotal mediator of Spns2/S1P signaling in modulating the immune response in macrophages, contributing to both the initial hyperinflammatory phase and subsequent immunosuppression.

Collaborative activation of S1PRs is necessary for mitochondrial functions in macrophages

Spns2/S1P signaling functions by triggering the activation of S1PR(s). However, the specific S1PR(s) responsible for modulating mitochondrial functions have not yet been elucidated. All five S1PRs were transcriptionally detectable in PMs, irrespective of the presence of Spns2. Among them, *S1pr1* and *S1pr2* exhibited high expression levels, whereas *S1pr3* showed the lowest abundance under basal conditions (Fig. 7A).

Next, we sought to investigate the potential impact of modulating S1PR activation on *Ptges* expression. In WT PMs, we selectively inhibited S1PR1-4 using the specific antagonists W146, JTE013, TY-52,156, and CYM50358, respectively [5, 32]. Unfortunately, an antagonist for S1PR5 was not available. The inhibition of each S1PR, particularly S1PR2, S1PR3, and S1PR4, led to increased expression of *Ptges* (Fig. 7B). Meanwhile, we observed similar but more pronounced upregulation of *PTGES* expression in THP-1 cells following S1PR inhibition (Supplementary Fig. 5A). Furthermore, the fluorescence intensities of MitoTracker™ Red, which are reliant on ΔΨm, decreased in each group (Fig. 7C, Supplementary Fig. 5B), while the fluorescence intensities of CytoFix™ MitoRed, which are independent of ΔΨm, exhibited an increase (Fig. 7D, Supplementary Fig. 5C). Intriguingly, despite the low abundance of gene expression,

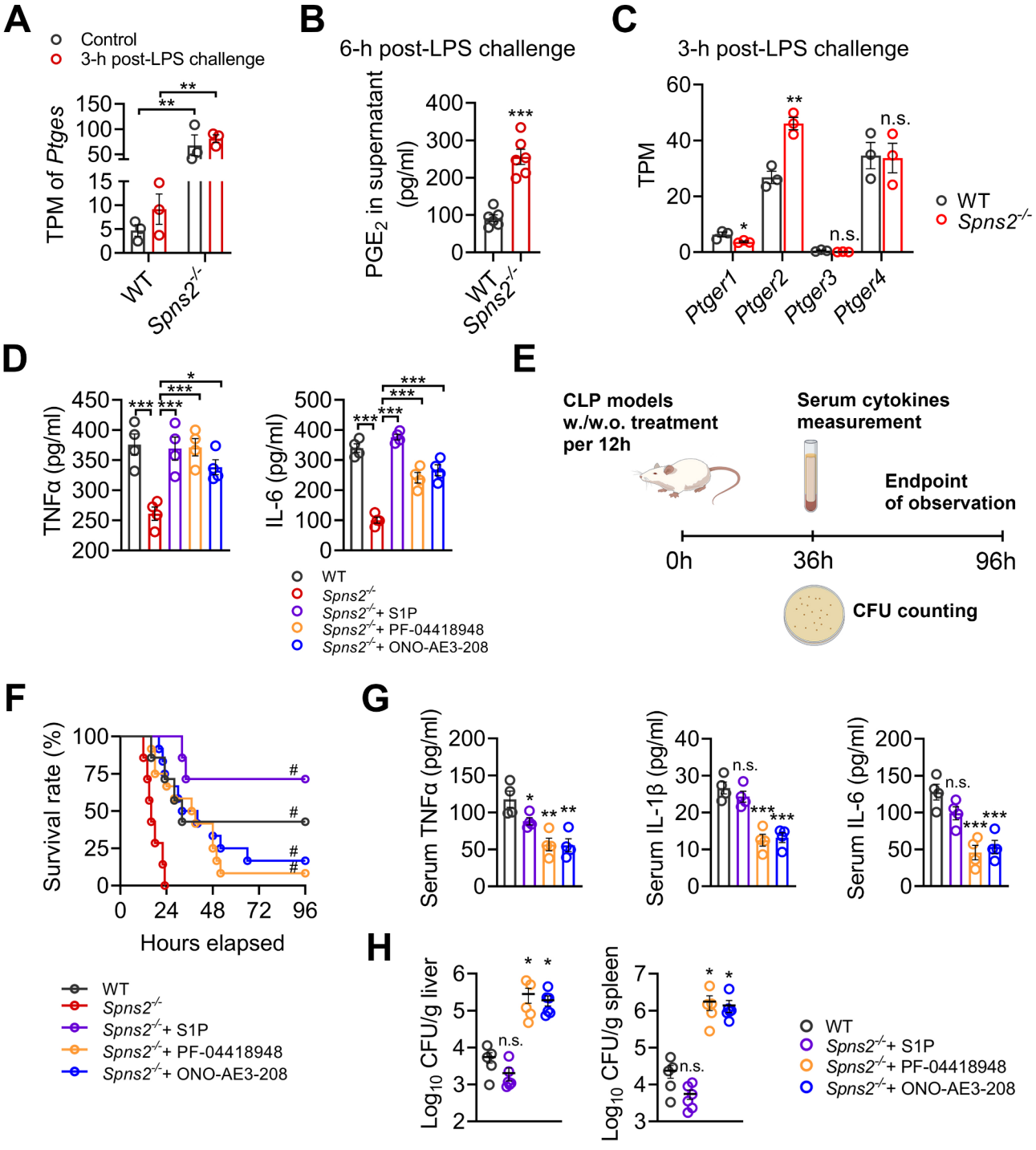

Fig. 6 Excessive PGE_2 production induces immunosuppression as infection progresses **(A)** *Spns2*$^{-/-}$ PMs exhibit significantly elevated gene expression of *Ptges* compared to WT PMs before and after the LPS challenge. TPM, transcripts per kilobase of exon model per million mapped reads. $N=3$ biological replicates. **(B)***Spns2*$^{-/-}$ PMs release higher levels of PGE_2 than WT PMs within 6-h post-LPS challenge. $N=6$ biological replicates. **(C)** Gene expression of E-type prostanoid receptors in PMs at 3-h post-LPS challenge. $N=3$ biological replicates. **(D)** Blockade of both EP2 and EP4 enhances TNFα and IL-6 release by *Spns2*$^{-/-}$ PMs within 12-h post-LPS challenge. $N=4$ biological replicates. **(E)** Schematic of the in vivo experiments using CLP models. **(F)** Survival curves from CLP models demonstrate that partial recovery of the inflammatory response induced by either EP2 or EP4 blockade improves the survival of *Spns2*$^{-/-}$ rats. $N=7$ to 12 biological replicates. **(G)** The levels of serum pro-inflammatory cytokines measured at 36-h post-infection indicate that EP2 or EP4 inhibition is effective but insufficient to overcome immunosuppression in *Spns2*$^{-/-}$ CLP models. $N=4$ biological replicates. **(H)** Colony-forming units (CFU) counts in livers and spleens at 36-h post-infection reveal higher bacterial loads in EP2- and EP4-inhibited *Spns2*$^{-/-}$ CLP models. $N=5$ to 6 biological replicates. Data are presented as mean ± s.e.m. (**A** to **D**, **G**, and **H**) and percentage **(F)**. *P* values were determined by unpaired *t*-test (**A** to **C**), one-way ANOVA with Sidak's correction for multiple comparisons (**D**, **G**, and **H**), and log-rank test adjusted by the Bonferroni method **(F)**. $^{*}P<0.05$; $^{**}P<0.01$; $^{***}P<0.001$; n.s., not significant. # indicates *P* value is less than the Bonferroni-corrected threshold

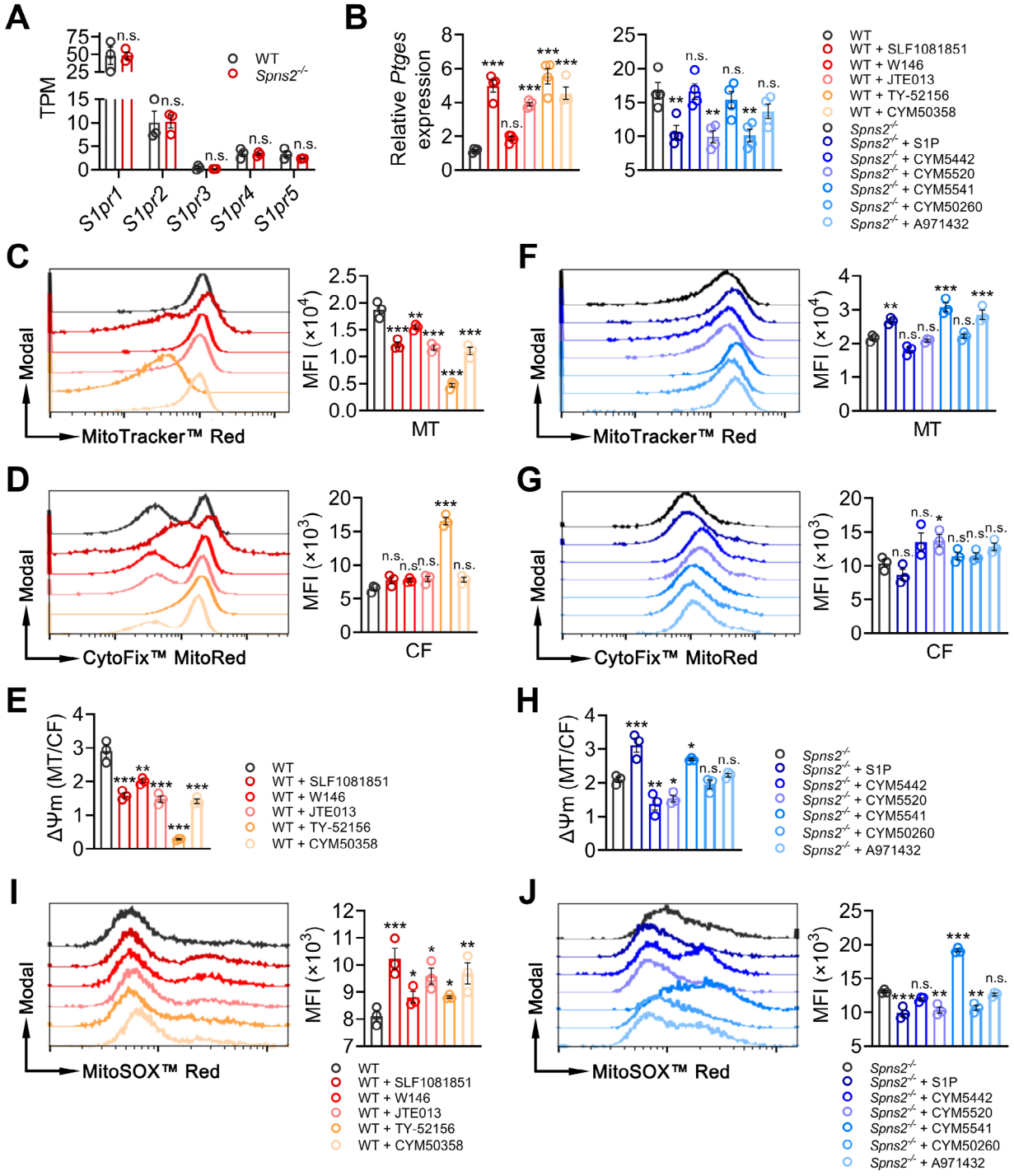

Fig. 7 Spns2/S1P signaling impacts mitochondrial functions through coordinated activation of multiple S1P receptors **(A)** All five S1PRs are transcriptionally detectable in PMs. $N=3$ biological replicates. **(B)** Inhibition of individual S1PRs in WT PMs increases the gene expression of *Ptges*, while activation of S1PR2 and S1PR4 in *Spns2*$^{-/-}$ PMs may slightly reduce *Ptges* expression. $N=4$ biological replicates. **(C)** In WT PMs, blocking individual S1PRs reduces the fluorescence intensity of MitoTracker™ Red, indicating diminished ΔΨm. **(D)** S1PR3 blockade significantly increases the fluorescence intensity of CytoFix™ MitoRed, indicating increased mitochondrial mass, while blockade of other receptors may cause a slight increase in mitochondrial mass. **(E)** All treatments result in reduced average Δψm (calculated by the ratio of MT/CF) in WT PMs. $N=3$ biological replicates (**C** to **E**). (**F**, **G**) In *Spns2*$^{-/-}$ PMs, activation of S1PR3 and S1PR5 increases MitoTracker™ Red fluorescence intensity **(F)**, but none of the treatments affect mitochondrial mass **(G)**. **(H)** Only S1PR3 activation partially restores the average Δψm in *Spns2*$^{-/-}$ PMs. $N=3$ biological replicates (**F** to **H**). **(I)** All the antagonists increase mtROS generation in WT PMs, especially with S1PR2 and S1PR4 blockade. $N=3$ biological replicates. **(J)** In *Spns2*$^{-/-}$ PMs, activation of S1PR2 and S1PR4 attenuates oxidative stress. $N=3$ biological replicates. Data are presented as mean ± s.e.m. *P* values were determined by unpaired *t*-test **(A)** and one-way ANOVA with Sidak's correction for multiple comparisons (**B** to **J**). *$P<0.05$; **$P<0.01$; ***$P<0.001$; n.s., not significant

blocking S1PR3 resulted in the most notable changes in the fluorescence intensities in WT PMs (Fig. 7C and D). In THP-1 cells, however, S1PR2 and S1PR4 appeared to be more predominant (Supplementary Fig. 5B and C). Consequently, the average ΔΨm decreased in each group (Fig. 7E, Supplementary Fig. 5D).

In *Spns2*$^{-/-}$ PMs, we employed the specific agonists CYM5442, CYM5520, CYM5541, CYM50260, and A971432 to activate S1PR1-5, respectively [5, 32–34]. The results indicated that the activation of S1PR2 and S1PR4 moderately reduced *Ptges* expression (Fig. 7B). However, despite S1PR3 and S1PR5 activation increasing MitoTracker™ Red fluorescence intensities (Fig. 7F), none of the S1PRs individually reduced mitochondrial mass as effectively as S1P treatment (Fig. 7G). As a result, only S1PR3 activation appeared to partially restore the average ΔΨm (Fig. 7H).

We also observed alterations in mtROS generation by manipulating S1PR activation. In WT PMs and THP-1 cells, the administration of antagonists led to elevated mtROS levels to varying degrees, with S1PR2 and S1PR4 inhibition being the most pronounced (Fig. 7I, Supplementary Fig. 5E). These findings generally aligned with the changes observed in *Ptges* expression and the average ΔΨm. In *Spns2*$^{-/-}$ PMs, S1PR activation attenuated oxidative stress, except for S1PR3 and S1PR5 (Fig. 7J). Overall, these results suggest that the impact of Spns2/S1P signaling on mitochondrial functions likely depends on the collective activation of different S1PRs rather than any single one.

Discussion

S1P is a crucial immunomodulatory molecule that impacts the progression of infections and autoimmune diseases and has been identified as a potential therapeutic target [35]. Several studies have investigated the roles of S1PR activation in macrophage immune response during bacterial infections. For instance, S1PR1 activation exerts an anti-inflammatory effect in LPS-challenged macrophages, leading to a reduced release of pro-inflammatory cytokines and nitric oxide production [36]. Furthermore, S1P induces NLRP3 inflammasome activation and ROS generation in LPS-primed macrophages via S1PR2 signaling [37]. In contrast to S1PR1, S1PR3 activation triggers a pro-inflammatory response and is essential for macrophages to drive bactericidal activity through ROS production [38, 39]. Recently, Ziegler et al.. demonstrated that during the acute phase of sepsis, inhibiting S1P lyase or activating S1PR3 effectively alleviates hyperinflammation and enhances lung barrier stability, thereby reducing the severity of sepsis and improving survival in mice [40, 41]. It is noteworthy that all five S1PRs are expressed in macrophages, despite differences in expression abundance before and after bacterial infections, suggesting potential cooperative functions [39]. In this study, we propose that all five S1PRs may contribute to shaping the mitochondrial functions of macrophages, which are closely linked to the immune response during bacterial infections [2, 4]. Previously, we demonstrated that macrophage Spns2/S1P signaling functions as a crucial metabolic modulator and affects the antibacterial response [6]. Here, we identify PGE_2 as the bridging molecule between Spns2/S1P signaling and mitochondrial respiration. These findings also elucidate why Spns2/S1P signaling plays roles in both the early hyperinflammatory stages and later immunosuppression of bacterial infections [10].

PGE_2 functions as an important mediator in macrophage-related inflammation, yet its comprehensive roles remain ambiguous due to conflicting reports of both pro- and anti-inflammatory activities in the context of bacterial infections [11]. For instance, PGE_2 has been shown to stimulate the expression of CD14, an LPS co-receptor, thereby enhancing the activation of Toll-like receptor 4 (TLR4) [19]. Additionally, PGE_2 amplifies IL-1β release triggered by NLRP3 inflammasome activation in LPS-primed macrophages [42]. Furthermore, PGE_2 impedes TLR4 internalization and associated TRIF signaling, sustaining the pro-inflammatory TLR4-MyD88 signaling cascade [43]. Notably, these findings primarily examined the effects of PGE_2 during the initial stages of macrophage activation, while studies concluding the anti-inflammatory properties of PGE_2 focus on its longer-term effects [17, 44, 45]. Consistently, our results demonstrate that excessive PGE_2 production contributes to both hyperinflammation within 3-h post-LPS challenge and subsequent immunosuppression in *Spns2*$^{-/-}$ PMs, implying that PGE_2 modulates inflammation in a time-dependent manner. Despite variations in the time points across studies, the broad concentration range of PGE_2 treatment from 10 to 1000 nM may also affect outcomes, as different receptors could be engaged under varying conditions [46].

Recent studies have reinforced the metabolic significance of PGE_2 in macrophages, affecting both homeostasis and immune functions. For example, elevated levels of PGE_2 in aged lungs inhibit the proliferation of alveolar macrophages by reducing OXPHOS and mitophagy, impairing the immune response to the influenza A virus [47]. Similarly, aged macrophages and microglia exhibit reduced mitochondrial respiration due to heightened activation of the PGE_2-EP2 pathway, resulting in sustained maladaptive inflammation and cognitive decline [48]. Therefore, targeting mitochondria emerges as a key mechanism by which PGE_2 influences macrophage state and functions. In the present study, we propose that Spns2/S1P serves as a critical regulator of PGE_2 signaling in macrophages. Spns2 deficiency leads to excessive

PGE_2 production and EP4 activation, resulting in compromised MAS function, decreased OXPHOS, elevated lactate-ROS axis activity, and hyperinflammation during the initial phases of bacterial infections. Additionally, Sanin et al.. have shown that PGE_2 instigates transcriptional suppression of MAS-related genes, leading to dissipated ΔΨm and altered chromatin accessibility in IL-4-activated macrophages [49]. Overall, augmenting Spns2/S1P signaling could be a promising strategy for regulating immune homeostasis, especially in cases of excessive PGE_2 activation.

To date, only a few studies have elucidated the link between extracellular S1P signaling and PGE_2 production. Johann et al.. reported that S1P derived from apoptotic cells (AC) stimulates PGE_2 production by stabilizing COX2 mRNA and enhancing protein expression in macrophages [50]. Additionally, Brecht et al.. found that S1PR1 and/or S1PR3 in macrophages may respond to AC-derived S1P, leading to increased PGE_2 production to facilitate angiogenesis [51]. However, the stimulatory effect of extracellular S1P on PGE_2 production is largely contingent upon the presence of other stimuli in an AC-conditioned medium, as S1P alone may not elicit PLA_2 activation or PGE_2 production [50]. These findings suggest that the impact of extracellular S1P on PGE_2 production may vary under distinct circumstances.

In summary, our study demonstrates that Spns2/S1P signaling plays a pivotal role in regulating mitochondrial functions and inflammatory response by modulating PGE_2 signaling in macrophages (Fig. 8). Effective Spns2/S1P signaling suppresses PGE_2 production, thereby preserving OXPHOS in resting macrophages. Conversely, excessive activation of the PGE_2-EP4 pathway impairs MAS activity and mitochondrial respiration, leading to intracellular lactate accumulation. During bacterial infections, elevated PGE_2 levels due to Spns2 deficiency drive early-phase hyperinflammation, partially through the overactivation of the lactate-ROS axis mediated by PGE_2-EP4. Prolonged exposure to high levels of PGE_2 triggers immunosuppression in later stages. These findings elucidate the interplay between Spns2/S1P signaling and PGE_2 production in macrophages, providing insight into a potential mechanism for the dual roles of Spns2/S1P signaling in maintaining immune homeostasis during bacterial infections.

Conclusions

Spns2/S1P signaling suppresses PGE_2 production by activating multiple S1PRs to sustain OXPHOS in macrophages. Elevated PGE_2 due to Spns2 deficiency impairs MAS activity and mitochondrial respiration, thereby intensifying the lactate-ROS axis and triggering

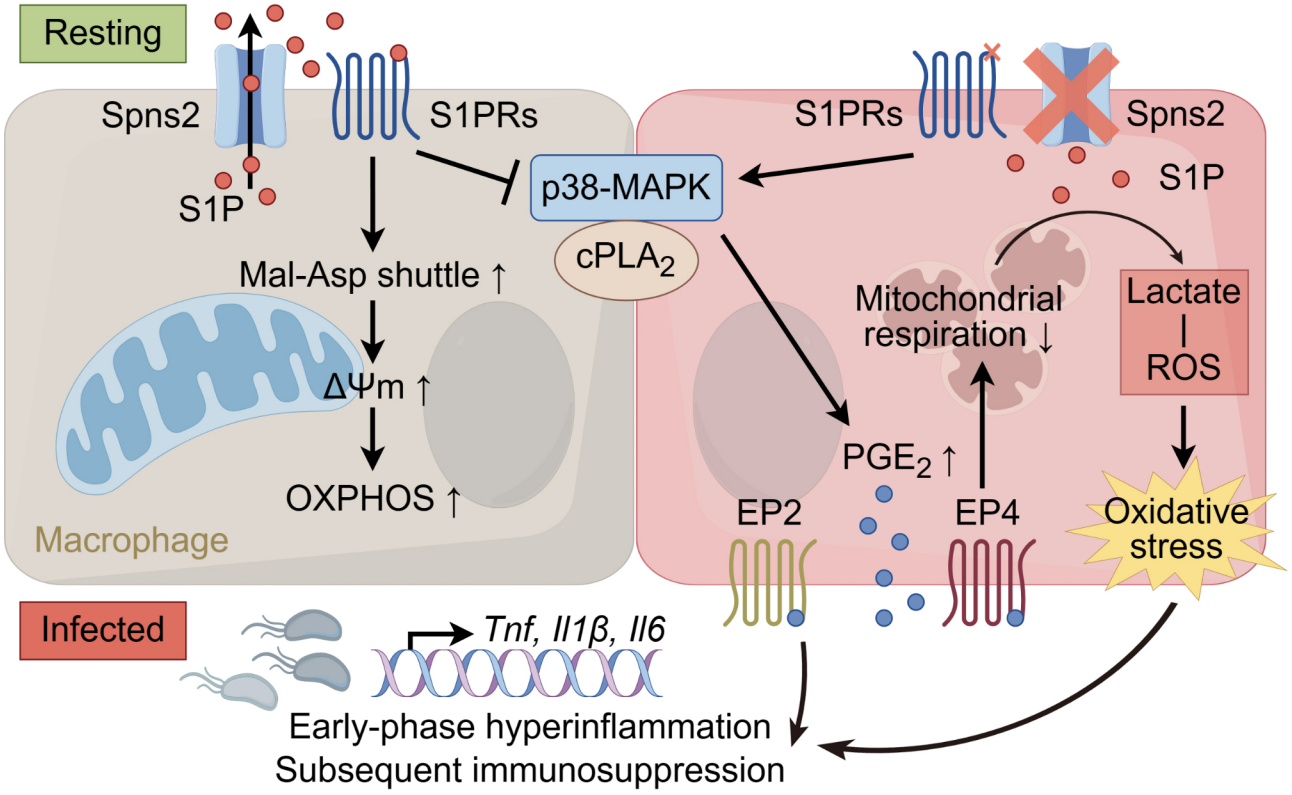

Fig. 8 Schematic illustration of how Spns2/S1P signaling modulates mitochondrial functions and inflammatory response through PGE_2 production in macrophages

hyperinflammation in the early phases of bacterial infections. Subsequently, PGE_2 induces immunosuppression, highlighting the dual roles of PGE_2 in modulating macrophage immune response during infections.

Abbreviations

Spns2	Spinster homolog 2
S1P	Sphingosine-1-phosphate
PGE_2	Prostaglandin E_2
MAS	Malate-aspartate shuttle
ROS	Reactive oxygen species
mtROS	mitochondrial reactive oxygen species
EP	E-type prostanoid receptor
OXPHOS	Oxidative phosphorylation
AA	Arachidonic acid
PLA_2	Phospholipase A_2
COX	Cyclooxygenase
mPGES	microsomal PGE synthase
cPGES	cytosolic PGE synthase
MAPK	Mitogen-activated protein kinase
PMs	Peritoneal macrophages
E. coli	Escherichia coli
CFU	Colony-forming units
CLP	Cecal ligation and puncture
ΔΨm	Mitochondrial membrane potential
OCR	Oxygen consumption rate
FCCP	Carbonyl cyanide-4-(trifluoromethoxy) phenylhydrazone
SOD	Superoxide dismutase
TLR	Toll-like receptor

Supplementary Information

The online version contains supplementary material available at https://doi.org/10.1186/s12964-024-01851-z.

Supplementary Material 1

Acknowledgements
The schematic illustrations in this study were created using Figdraw.

Author contributions
CF, XZ, JL, and ML planned the project and wrote the original draft. CF, PR, YH, and YW conducted the investigation process. SY and CZ validated, analyzed, and visualized the data. XL reviewed and revised the manuscript. All authors read and approved the final manuscript.

Funding
This work was supported by grants from the National Natural Science Foundation of China (81903671 and 31570986).

Data availability
The raw data of untargeted metabolite profilings have been deposited in the MetaboLights database (https://www.ebi.ac.uk/metabolights) with the accession MTBLS9920. The raw data of RNA-seq have been deposited in the Sequence Read Archive (SRA) database with the accession PRJNA904828.

Declarations

Ethics approval and consent to participate
Ethical approval for all experimental procedures was obtained from the Animal Care and Use Committee of the Fourth Military Medical University.

Consent for publication
Not applicable.

Competing interests
The authors declare no competing interests.

Author details
[1]Department of Pharmacology, School of Pharmacy, Fourth Military Medical University, Xi'an, China
[2]Department of Burns and Plastic Surgery, Tangdu Hospital, Fourth Military Medical University, Xi'an, China
[3]Department of Plastic Surgery, Xijing Hospital, Fourth Military Medical University, Xi'an, China
[4]Department of Burns, Plastic and Wound Repair Surgery, the Second Affiliated Hospital, Xi'an Jiaotong University, Xi'an, China

Received: 2 June 2024 / Accepted: 23 September 2024
Published online: 30 September 2024

References

1. Caputa G, Castoldi A, Pearce EJ. Metabolic adaptations of tissue-resident immune cells. Nat Immunol. 2019;20:793–801.
2. Almeida L, Dhillon-LaBrooy A, Sparwasser T. The evolutionary tug-of-war of macrophage metabolism during bacterial infection. Trends Endocrinol Metab. 2024;35:235–48.
3. Gleeson LE, Sheedy FJ. Metabolic reprogramming & inflammation: fuelling the host response to pathogens. Semin Immunol. 2016;28:450–68.
4. Gauthier T, Chen W. Modulation of macrophage immunometabolism: a New Approach to fight infections. Front Immunol. 2022;13:780839.
5. Mohammed S, Bindu A, Viswanathan A, Harikumar KB. Sphingosine 1-phosphate signaling during infection and immunity. Prog Lipid Res. 2023;92:101251.
6. Fang C, Ren P, Bian G, Wang J, Bai J, Huang J, Ding Y, Li X, Li M, Hou Z. Enhancing Spns2/S1P in macrophages alleviates hyperinflammation and prevents immunosuppression in sepsis. EMBO Rep. 2023;24:e56635.
7. Borst P. The malate-aspartate shuttle (Borst cycle): how it started and developed into a major metabolic pathway. IUBMB Life. 2020;72:2241–59.
8. Wang Y, Stancliffe E, Fowle-Grider R, Wang R, Wang C, Schwaiger-Haber M, Shriver LP, Patti GJ. Saturation of the mitochondrial NADH shuttles drives aerobic glycolysis in proliferating cells. Mol Cell. 2022;82:3270–e32833279.
9. Willems PH, Rossignol R, Dieteren CE, Murphy MP, Koopman WJ. Redox Homeostasis and mitochondrial dynamics. Cell Metab. 2015;22:207–18.
10. Vanderhaeghen T, Vandewalle J, Libert C. Spns2/S1P: it takes two to tango with inflammation and metabolic rewiring during sepsis. EMBO Rep. 2023;24:e57615.
11. Martinez-Colon GJ, Moore BB. Prostaglandin E(2) as a Regulator of immunity to pathogens. Pharmacol Ther. 2018;185:135–46.
12. Murakami M. The phospholipase A(2) superfamily as a central hub of bioactive lipids and beyond. Pharmacol Ther. 2023;244:108382.
13. Weigert A, Strack E, Snodgrass RG, Brune B. mPGES-1 and ALOX5/-15 in tumor-associated macrophages. Cancer Metastasis Rev. 2018;37:317–34.
14. Mortimer L, Moreau F, MacDonald JA, Chadee K. NLRP3 inflammasome inhibition is disrupted in a group of auto-inflammatory disease CAPS mutations. Nat Immunol. 2016;17:1176–86.
15. Sokolowska M, Chen LY, Liu Y, Martinez-Anton A, Qi HY, Logun C, Alsaaty S, Park YH, Kastner DL, Chae JJ, Shelhamer JH. Prostaglandin E2 inhibits NLRP3 inflammasome activation through EP4 receptor and intracellular cyclic AMP in human macrophages. J Immunol. 2015;194:5472–87.
16. Pereira M, Liang J, Edwards-Hicks J, Meadows AM, Hinz C, Liggi S, Hepprich M, Mudry JM, Han K, Griffin JL, et al. Arachidonic acid inhibition of the NLRP3 inflammasome is a mechanism to explain the anti-inflammatory effects of fasting. Cell Rep. 2024;43:113700.
17. Fleming BD, Chandrasekaran P, Dillon LA, Dalby E, Suresh R, Sarkar A, El-Sayed NM, Mosser DM. The generation of macrophages with anti-inflammatory activity in the absence of STAT6 signaling. J Leukoc Biol. 2015;98:395–407.
18. Martinez-Colon GJ, Taylor QM, Wilke CA, Podsiad AB, Moore BB. Elevated prostaglandin E(2) post-bone marrow transplant mediates interleukin-1beta-related lung injury. Mucosal Immunol. 2018;11:319–32.
19. Iwahashi H, Takeshita A, Hanazawa S. Prostaglandin E2 stimulates AP-1-mediated CD14 expression in mouse macrophages via cyclic AMP-dependent protein kinase A. J Immunol. 2000;164:5403–8.
20. Fang C, Bian GL, Ren P, Xiang J, Song J, Yu CY, Zhang Q, Liu L, Chen K, Liu FF, et al. S1P transporter SPNS2 regulates proper postnatal retinal morphogenesis. Faseb J. 2018;32:3597–613.

21. Bian GL, Yu CY, Liu L, Fang C, Chen K, Ren P, Zhangs Q, Liu FF, Zhang K, Xue Q et al. Sphingosine 1-phosphate stimulates eyelid closure in the developing rat by stimulating EGFR signaling. Sci Signal. 2018; 11:eaat1470.
22. af Forselles KJ, Root J, Clarke T, Davey D, Aughton K, Dack K, Pullen N. In vitro and in vivo characterization of PF-04418948, a novel, potent and selective prostaglandin EP(2) receptor antagonist. Br J Pharmacol. 2011;164:1847–56.
23. Toyoda Y, Morimoto K, Suno R, Horita S, Yamashita K, Hirata K, Sekiguchi Y, Yasuda S, Shiroishi M, Shimizu T, et al. Ligand binding to human prostaglandin E receptor EP(4) at the lipid-bilayer interface. Nat Chem Biol. 2019;15:18–26.
24. Rios FJ, Touyz RM, Montezano AC. Isolation and differentiation of murine macrophages. Methods Mol Biol. 2017;1527:297–309.
25. Yu W, Wang X, Zhao J, Liu R, Liu J, Wang Z, Peng J, Wu H, Zhang X, Long Z, et al. Stat2-Drp1 mediated mitochondrial mass increase is necessary for pro-inflammatory differentiation of macrophages. Redox Biol. 2020;37:101761.
26. Haeggstrom JZ. Leukotriene biosynthetic enzymes as therapeutic targets. J Clin Invest. 2018;128:2680–90.
27. Xie JH, Li YY, Jin J. The essential functions of mitochondrial dynamics in immune cells. Cell Mol Immunol. 2020;17:712–21.
28. Quintana-Cabrera R, Scorrano L. Determinants and outcomes of mitochondrial dynamics. Mol Cell. 2023;83:857–76.
29. Head B, Griparic L, Amiri M, Gandre-Babbe S, van der Bliek AM. Inducible proteolytic inactivation of OPA1 mediated by the OMA1 protease in mammalian cells. J Cell Biol. 2009;187:959–66.
30. Kraus F, Roy K, Pucadyil TJ, Ryan MT. Function and regulation of the divisome for mitochondrial fission. Nature. 2021;590:57–66.
31. Birukova AA, Zagranichnaya T, Fu P, Alekseeva E, Chen W, Jacobson JR, Birukov KG. Prostaglandins PGE(2) and PGI(2) promote endothelial barrier enhancement via PKA- and Epac1/Rap1-dependent rac activation. Exp Cell Res. 2007;313:2504–20.
32. Perez-Jeldres T, Alvarez-Lobos M, Rivera-Nieves J. Targeting Sphingosine-1-Phosphate Signaling in Immune-mediated diseases: beyond multiple sclerosis. Drugs. 2021;81:985–1002.
33. Onuma T, Tanabe K, Kito Y, Tsujimoto M, Uematsu K, Enomoto Y, Matsushima-Nishiwaki R, Doi T, Nagase K, Akamatsu S, et al. Sphingosine 1-phosphate (S1P) suppresses the collagen-induced activation of human platelets via S1P4 receptor. Thromb Res. 2017;156:91–100.
34. Satsu H, Schaeffer MT, Guerrero M, Saldana A, Eberhart C, Hodder P, Cayanan C, Schurer S, Bhhatarai B, Roberts E, et al. A sphingosine 1-phosphate receptor 2 selective allosteric agonist. Bioorg Med Chem. 2013;21:5373–82.
35. Sun G, Wang B, Wu X, Cheng J, Ye J, Wang C, Zhu H, Liu X. How do sphingosine-1-phosphate affect immune cells to resolve inflammation? Front Immunol. 2024;15:1362459.
36. Hughes JE, Srinivasan S, Lynch KR, Proia RL, Ferdek P, Hedrick CC. Sphingosine-1-phosphate induces an antiinflammatory phenotype in macrophages. Circ Res. 2008;102:950–8.
37. Lee CH, Choi JW. S1P/S1P(2) Signaling Axis regulates both NLRP3 upregulation and NLRP3 inflammasome activation in Macrophages primed with Lipopolysaccharide. Antioxid (Basel). 2021; 10:1706.
38. Hou J, Chen Q, Wu X, Zhao D, Reuveni H, Licht T, Xu M, Hu H, Hoeft A, Ben-Sasson SA, et al. S1PR3 Signaling drives bacterial killing and is required for survival in bacterial Sepsis. Am J Respir Crit Care Med. 2017;196:1559–70.
39. Heo JY, Im DS. Pro-inflammatory role of S1P(3) in macrophages. Biomol Ther (Seoul). 2019;27:373–80.
40. Ziegler AC, Haider RS, Hoffmann C, Graler MH. S1PR3 agonism and S1P lyase inhibition rescue mice in the severe state of experimental sepsis. Biomed Pharmacother. 2024;174:116575.
41. Weigel C, Huttner SS, Ludwig K, Krieg N, Hofmann S, Schroder NH, Robbe L, Kluge S, Nierhaus A, Winkler MS, et al. S1P lyase inhibition protects against sepsis by promoting disease tolerance via the S1P/S1PR3 axis. EBioMedicine. 2020;58:102898.
42. Hua KF, Chou JC, Ka SM, Tasi YL, Chen A, Wu SH, Chiu HW, Wong WT, Wang YF, Tsai CL, et al. Cyclooxygenase-2 regulates NLRP3 inflammasome-derived IL-1beta production. J Cell Physiol. 2015;230:863–74.
43. Perkins DJ, Richard K, Hansen AM, Lai W, Nallar S, Koller B, Vogel SN. Autocrine-paracrine prostaglandin E(2) signaling restricts TLR4 internalization and TRIF signaling. Nat Immunol. 2018;19:1309–18.
44. Degraaf AJ, Zaslona Z, Bourdonnay E, Peters-Golden M. Prostaglandin E2 reduces toll-like receptor 4 expression in alveolar macrophages by inhibition of translation. Am J Respir Cell Mol Biol. 2014;51:242–50.
45. Cilenti F, Barbiera G, Caronni N, Iodice D, Montaldo E, Barresi S, Lusito E, Cuzzola V, Vittoria FM, Mezzanzanica L, et al. A PGE(2)-MEF2A axis enables context-dependent control of inflammatory gene expression. Immunity. 2021;54:1665–e16821614.
46. Norel X, Sugimoto Y, Ozen G, Abdelazeem H, Amgoud Y, Bouhadoun A, Bassiouni W, Goepp M, Mani S, Manikpurage HD, et al. International Union of Basic and Clinical Pharmacology. CIX. Differences and similarities between Human and Rodent Prostaglandin E(2) receptors (EP1-4) and prostacyclin receptor (IP): specific roles in pathophysiologic conditions. Pharmacol Rev. 2020;72:910–68.
47. Chen J, Deng JC, Zemans RL, Bahmed K, Kosmider B, Zhang M, Peters-Golden M, Goldstein DR. Age-induced prostaglandin E(2) impairs mitochondrial fitness and increases mortality to influenza infection. Nat Commun. 2022;13:6759.
48. Minhas PS, Latif-Hernandez A, McReynolds MR, Durairaj AS, Wang Q, Rubin A, Joshi AU, He JQ, Gauba E, Liu L, et al. Restoring metabolism of myeloid cells reverses cognitive decline in ageing. Nature. 2021;590:122–.
49. Sanin DE, Matsushita M, Geltink RIK, Grzes KM, Bakker NV, Corrado M, Kabat AM, Buck MD, Qiu J, Lawless SJ, et al. Mitochondrial membrane potential regulates Nuclear Gene expression in Macrophages exposed to Prostaglandin E2. Immunity. 2018;49:1021–.
50. Johann AM, Weigert A, Eberhardt W, Kuhn AM, Barra V, von Knethen A, Pfeilschifter JM, Brüne B. Apoptotic cell-derived sphingosine-1-phosphate promotes HuR-dependent cyclooxygenase-2 mRNA stabilization and protein expression. J Immunol. 2008;180:1239–48.
51. Brecht K, Weigert A, Hu J, Popp R, Fisslthaler B, Korff T, Fleming I, Geisslinger G, Brüne B. Macrophages programmed by apoptotic cells promote angiogenesis via prostaglandin E2. Faseb J. 2011;25:2408–17.

Publisher's note